# Supporting Information

Supporting Information for the paper entitled "Anomalous stability of graphene containing defects covered by a water layer" by Ruixia Song, Sonam Wangmo, Minsi Xin, Yan Meng, Ping Huai, Zhigang Wang * and Ruiqin Zhang *



## 1. Configuration selection of the defective graphene

In order to select the most stable defective graphene model as the initial structure of the water adsorption system, we have performed structural optimizations of graphene models with different numbers of defects, which are used to select the one of the lowest energy as the initial structure. The detailed processes are shown in Figure S1, Figure S2 and S3, respectively.

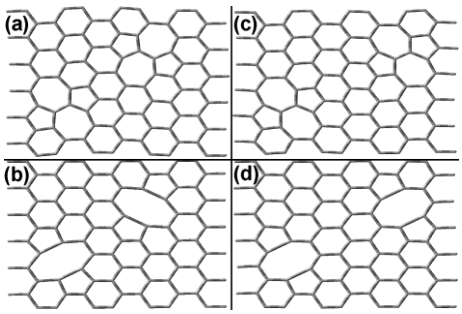


Figure S1. The configurations of two Stone-Wales and two $C_2$ vacancy defects in graphene. The selected configurations of defective graphene models shown in Figure (a) and (b) are of total energies of -166.290 Hatree and -159.151 Hatree, respectively; the total energies of the other two configurations in Figure (c) and (d) are -166.153 Hatree and -159.06 Hatree.

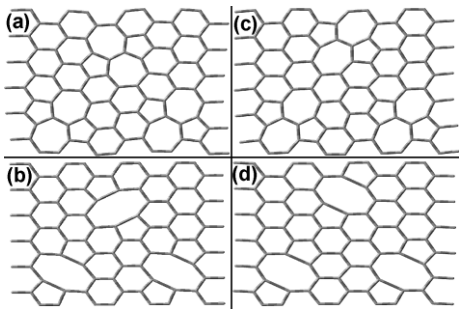


Figure S2. The configurations of three Stone-Wales and three $C_2$ vacancy defects in graphene. The selected configurations of defective graphene models shown in Figure (a) and (b) are of total energies of -166.109 Hatree and -155.410 Hatree, respectively; the total energies of the other two configurations in Figure (c) and (d) are -165.895 Hatree and -155.266 Hatree.

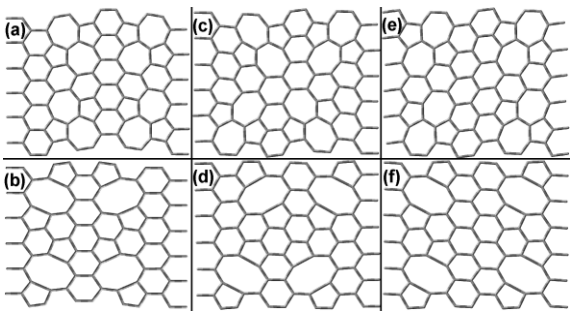

Figure S3. The configurations of four Stone-Wales and four $C_2$ vacancy defects in graphene. The selected configurations of the defective graphene models shown in Figure (a) and (b) are of their total energy of -165.888 Hatree and -151.588 Hatree, respectively; the total energies of the middle two configurations in Figure (c) and (d) are -165.547 Hatree and -151.453 Hatree; the total energies of the last two configurations in Figure (e) and (f) are -165.642 Hatree and -151.468 Hatree.

## 2. The transition point of the system tending to reach a dynamic equilibrium with time evolution

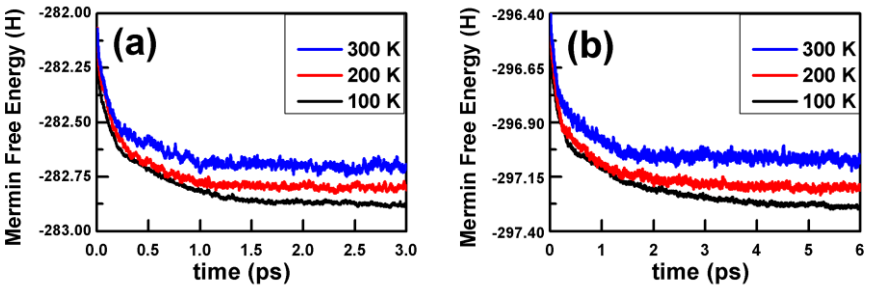


Figure S4. Free energy comparison under the different temperatures and with the same kinds of defects for (a) the water layer on 4 $C_2$ vacancy defects at 100 K, 200 K and 300 K; (b) the water layer on 4 Stone-Wales defects at 100 K, 200 K and 300 K.

In Figure S4 (a) and (b) the simulations are at different temperatures. The results indicate that the temperature affects the transition point of the system tending to reach dynamic equilibrium. As the temperature increases, the system reaches dynamic equilibrium earlier. Similar observation has been reported in Ref. 21.

## 3. The IR vibrational spectra of the three types of water-graphene systems

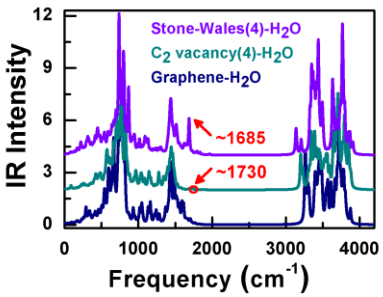


Figure S5. (Color online) IR spectra of the three types of water-graphene systems. The characteristic vibrational modes of Stone-Wales defects and $C_2$ vacancy defects which are indicated with arrows at about 1685 $cm^{-1}$ for formaer and at about 1730 $cm^{-1}$ for latter respectively.

We also analyzed the IR vibrational spectra of water-graphene adsorption systems shown in Figure S5. The curves from bottom to top represent the IR spectra of a single water layer on the perfect graphene, on the graphene with four $C_2$ vacancy defects, and on the graphene with 4 Stone Wales defects, respectively. We note that the calculation accuracy of DFTB and the presence of the water layer may cause a certain degree of uncetainty in the result. Nevertheless, we still observed the vibrational modes relating to Stone-Wales and $C_2$ vacancy defects, at around 1685 $cm^{-1}$ and 1730 $cm^{-1}$, respectively. The result is in qualitative agreement with the previous report on vibration spectra of the two types of defects[S1].

## 4. The density of states of the graphene containing 1, 2 or 3 defects

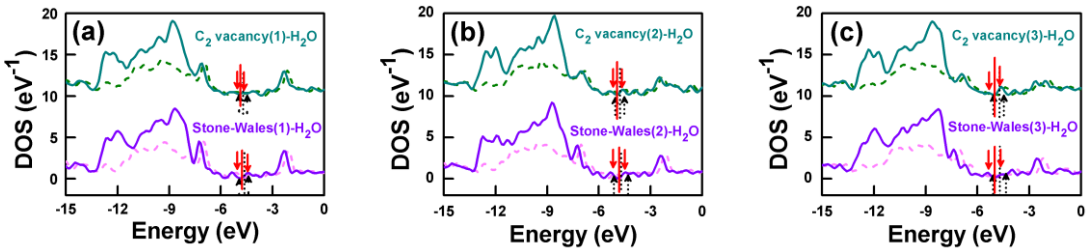


Figure S6. Density of states of graphenes with different number defects adsorbed with (solid line) and without (dotted line) a water layer. (a) 1 defect, (b) 2 defects, (c) 3 defects. There are similar peaks and shift trends as described in the text.

## 5. The distribution diagram of charge density

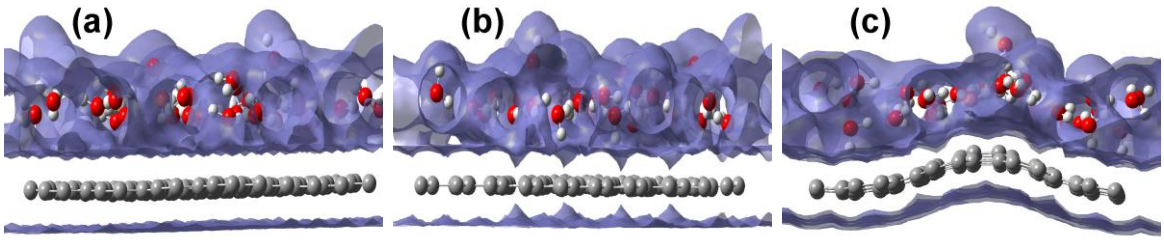


Figure S7. The charge density distribution of the water layer adsorbed on the perfect graphene, and on the graphene with 4 $C_2$ vacancy and 4 Stone-Wales defects, respectively. (a) the perfect graphene; (b) the case of 4 $C_2$ vacancy defects; and (c) the case of 4 Stone-Wales defects.

Figure S7 shows the charge distributed around the water molecules and the carbon atoms of the graphene. The charge distribution remained essentially planner at the bottom of $C_2$ vacancy defects compared with that in the perfect graphene. Due to the absence of two atoms at the vacancy position, there is a slight protrusion at the defect location (4 small protrusions in Figure S7 (b)). Unlike the other, the charge distribution renders folding bending with defect deformation for the graphene with four Stone-Wales defects.

## 6. The orbitals corresponding to the DOS peak position of the three kinds of water systems

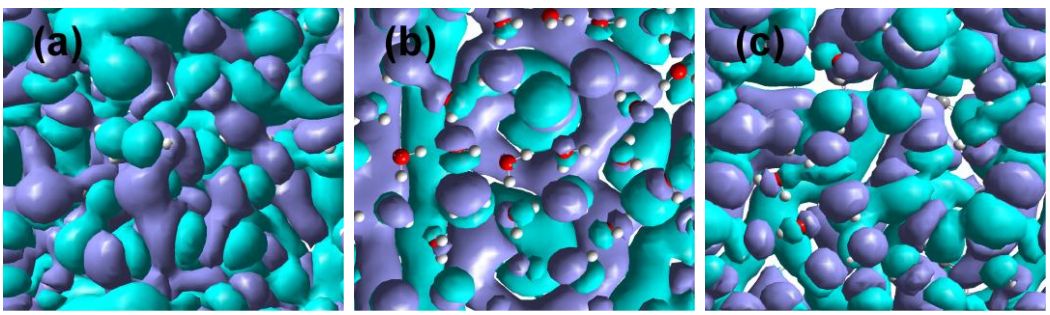


Figure S8. (Color online) The molecular orbits of water layer adsorbed on graphene corresponding to the peak of DOS (see the text for details) for the water layer on: (a) the graphene with 4 Stone-Wales defects; (b) the graphene with 4 $C_2$ vacancy defects; and (c) the perfect graphene.

Based on Figure 5, the adsorption of the single water layer generates some new peaks obviously. To further understand the origin of typical peaks in the case of water adsorption, we draw the orbitals corresponding to the peak position of the three kinds of water systems in Figure S8, these orbitals have obvious dumbbell-shaped orbital characteristics of the p electrons. It can be seen that these peaks are mainly contributed by the p-orbital of O atoms and C atoms.

## 7. References for Supporting Information

S1 M. S. Xin, F. T. Wang, Y. Meng, C. J. Tian, M. X. Jin, Z. G. Wang, and R. Q. Zhang, *J. Phys. Chem. C*, **2012**, *116*, 292-297.